

# Directed flow in a baryonic fireball

Tribhuban Parida\* and Sandeep Chatterjee†

*Department of Physical Sciences,  
Indian Institute of Science Education and Research Berhampur,  
Transit Campus (Govt ITI),  
Berhampur-760010, Odisha, India*

## Abstract

Directed flow of identified hadrons in a baryon rich fireball is an interesting observable as it is expected to probe several physics aspects: the initial three dimensional baryon profile in the thermalised fireball that can be treated as an input for the hydrodynamic evolution, the nature of baryon dissipation current and baryon transport coefficients, the QCD equation of state at finite baryon densities as well as the nature of phase transition between the quark gluon and hadronic phases. Particularly, the mid-rapidity slope of the rapidity dependence of directed flow of protons have been proposed as a sensitive observable to several of these physics aspects while a consistent description of the splitting in directed flow of baryon and its anti-particle has been a challenge. In this work, we propose a suitable ansatz of the initial condition for baryon deposition. When such a baryon deposition ansatz is coupled to a tilted fireball, we manage to find parameter space that can describe the directed flow of identified hadrons including the elusive baryon antibaryon splitting of directed flow. Further, we demonstrate that future measurements of baryon antibaryon directed flow at larger rapidities have the potential to constrain the baryon diffusion coefficient.

## I. INTRODUCTION

A large amount of energy as well as baryon and electric charges are deposited as a result of a relativistic heavy ion collision [1]. The framework of relativistic hydrodynamics has been very successful in evolving these conserved quantities with a few unknown parameters that characterise the initial thermalised distribution of these conserved quantities to be evolved hydrodynamically as well as the transport coefficients of these charges in the QCD medium. While the evolution of a baryon free fireball within the ambit of the above paradigm has been well studied and compared to appropriate observables for about two decades, hydrodynamic evolution of baryonic fireball is relatively new and pose several questions that are being understood. In this work we focus on the suitable thermalised distribution of the baryon density that can be evolved hydrodynamically and its consequences on observables that can be measured and tested. Directed flow of identified hadrons and particularly, the splitting of directed flow of baryons and anti-baryons have been well studied in this regard.

## II. MODEL

### A. Initial condition

The following ansatz has been taken for initial energy density  $\epsilon(x, y, \eta_s; \tau_0)$  at a constant proper time  $\tau_0$  [2].

$$\epsilon(x, y, \eta_s) = \epsilon_0 [(N_+(x, y)f_+(\eta_s) + N_-(x, y)f_-(\eta_s)) \times (1 - \alpha) + N_{coll}(x, y)\epsilon_{\eta_s}(\eta_s)\alpha] \quad (1)$$

$N_+(x, y)$  and  $N_-(x, y)$  are the participants from the forward and backward going nuclei respectively.  $N_{coll}(x, y)$  is the contribution from binary collision sources at the transverse position  $(x, y)$ .  $\alpha$  is the hardness factor. The rapidity odd component has been introduced through  $f_{+,-}(\eta_s)$  in  $\epsilon$ .

$$f_{+,-}(\eta_s) = \epsilon_{\eta_s}(\eta_s)\epsilon_{F,B}(\eta_s) \quad (2)$$

where

$$\epsilon_F(\eta_s) = \begin{cases} 0, & \text{if } \eta_s < -\eta_m \\ \frac{\eta_s + \eta_m}{2\eta_m}, & \text{if } -\eta_m \leq \eta_s \leq \eta_m \\ 1, & \text{if } \eta_m < \eta_s \end{cases} \quad (3)$$

and

$$\epsilon_B(\eta_s) = \epsilon_F(-\eta_s) \quad (4)$$

The initial baryon profile is modelled as,

$$n_B(x, y, \eta_s) = N_B [W_+^B(x, y)f_+^B(\eta_s) + W_-^B(x, y)f_-^B(\eta_s)] \quad (5)$$

where  $N_B$  is a normalisation constant to be determined from the condition that the total baryon deposited should be equal to the total participants  $N_{part} = N_+ + N_-$

$$\int \tau_0 dx dy d\eta n_B(x, y, \eta, \tau_0) = N_{part} \quad (6)$$

\* tribhubanp18@iiserbpr.ac.in

† sandeep@iiserbpr.ac.in

$W_{\pm}^B(x, y)$  are the weight factors to deposit baryon in the transverse plane and are taken to be of 2 component form

$$W_{\pm}^B(x, y) = (1 - \omega) N_{\pm}(x, y) + \omega N_{coll}(x, y) \quad (7)$$

This ansatz is quite different from the usual practice where the baryon transverse profile is taken to be proportional to  $N_{\pm}$  and contribution from binary collision sources is not considered [3]. Here we are motivated by microscopic, dynamical models like LEXUS [4, 5] where the baryon deposition in the initial state depends on the number of binary collisions. We keep  $\omega$  as a free parameter that can be tuned by comparing to data.

The net baryon density rapidity profiles  $f_{+}^{n_B}$ ,  $f_{-}^{n_B}$  are taken as [3, 6],

$$f_{+}^{n_B}(\eta_s) = \left[ \theta(\eta_s - \eta_0^{n_B}) \exp - \frac{(\eta_s - \eta_0^{n_B})^2}{2\sigma_{B,+}^2} + \theta(\eta_0^{n_B} - \eta_s) \exp - \frac{(\eta_s - \eta_0^{n_B})^2}{2\sigma_{B,-}^2} \right] \quad (8)$$

and

$$f_{-}^{n_B}(\eta_s) = \left[ \theta(\eta_s + \eta_0^{n_B}) \exp - \frac{(\eta_s + \eta_0^{n_B})^2}{2\sigma_{B,-}^2} + \theta(-\eta_s - \eta_0^{n_B}) \exp - \frac{(\eta_s + \eta_0^{n_B})^2}{2\sigma_{B,+}^2} \right] \quad (9)$$

The above profiles are constrained by comparing to rapidity dependence of net proton yield [1, 7–9]. In this paper, we work with an ensemble averaged initial profile of energy and baryon density by smearing the participant and binary collision sources obtained from event by event Monte-Carlo Glauber model of over 25,000 initial configurations from a given centrality class. In each event, first all the sources are rotated by the second order participant plane angle and then smeared around the new transverse position by a gaussian profile with constant transverse width of 0.4 fm [3]. The ensemble averaged profile is hydrodynamically evolved.

## B. Hydrodynamic Evolution

We evolve the initial energy and baryon densities from Eqs. 1 and 5 using the publicly available code MUSIC [10–12]. The code solves the following conservation equations

$$\partial_{\mu} T^{\mu\nu} = 0 \quad (10)$$

$$\partial_{\mu} J_B^{\mu} = 0 \quad (11)$$

The energy momentum tensor ( $T^{\mu\nu}$ ) and baryon current ( $J_B^{\mu}$ ) are defined as

$$T^{\mu\nu} = \epsilon u^{\mu} u^{\nu} - (p + \Pi) \Delta^{\mu\nu} + \pi^{\mu\nu} = 0 \quad (12)$$

$$J_B^{\mu} = n_B u^{\mu} + q^{\mu} \quad (13)$$

Here  $\Delta^{\mu\nu}$  is the spatial projection tensor defined as  $\Delta^{\mu\nu} = g^{\mu\nu} - u^{\mu} u^{\nu}$ , where  $u^{\mu}$  is the fluid four velocity and  $g^{\mu\nu} = \text{diag}(1, -1, -1, -1)$  is the metric tensor in Minkowski space.  $\epsilon$  and  $p$  are the local energy density and pressure in the fluid.  $T^{\mu\nu}$  and  $J_B^{\mu}$  consist of three dissipative currents, the bulk viscous pressure  $\Pi$ , the shear stress tensor  $\pi^{\mu\nu}$  and net baryon diffusion current  $q^{\mu}$  among which we do not consider the effect of  $\Pi$  in this work.

Like  $\pi^{\mu\nu}$ , the evolution of baryon diffusion current follows the Israel-Stewart-like equation.

$$\Delta^{\mu\nu} D q_{\nu} = - \frac{1}{\tau_q} \left( q^{\mu} - \kappa_B \nabla^{\mu} \frac{\mu_B}{T} \right) - \frac{\delta_{qq}}{\tau_q} q^{\mu} \theta - \frac{\lambda_{qq}}{\tau_q} q_{\nu} \sigma^{\mu\nu} \quad (14)$$

The above equation is a relaxation type equation where  $D = u^{\alpha} \partial_{\alpha}$  is the comoving time derivative.  $\tau_q$  is the time scale for the baryon diffusion current to relax to its Navier-Stokes limit chosen to be inversely proportional to the temperature  $T$  as in a conformal system.  $\delta_{qq}$  and  $\lambda_{qq}$  are the second order transport coefficients present in the coupling terms with velocity shear tensor  $\sigma^{\mu\nu}$  and system expansion rate  $\theta$ .

MUSIC uses a temperature ( $T$ ) and baryon chemical potential ( $\mu_B$ ) dependent baryon transport coefficient which is derived from Boltzman equation in relaxation time approximation [6].

$$\kappa_B = \frac{C_B}{T} n_B \left[ \frac{1}{3} \coth \left( \frac{\mu_B}{T} \right) - \frac{n_B T}{\epsilon + p} \right] \quad (15)$$

$C_B$  is a free parameter to control the strength of baryon diffusion in the medium.

A lattice QCD based EoS at finite baryon density, N<sub>EoS</sub>-BQS [13–16] has been used during the hydrodynamic evolution. The EoS imposes strangeness neutrality and fixed electric charge to baryon density ratio:  $n_Q = 0.4 n_B$ . We have taken the specific shear viscosity ( $C_{\eta} = \frac{\eta T}{\epsilon + p}$ ) to be 0.08 in the simulation.

The Cooper-Frye conversion of fluid into particles has been performed on the hypersurface of constant energy density,  $\epsilon_f = 0.26$  GeV/fm<sup>3</sup> using iSS [17, 18]. The sampled primary hadrons are then fed into UrQMD [19, 20] for hadronic transport.

## III. TILTED MATTER AND BARYON

The introduction of a 2 component transverse baryon profile in Eq. 7 allows us to tune the relative tilt between the matter and baryon profiles in the initial condition by varying  $\omega$ . This is demonstrated in Fig. 1. Contours of

constant baryon density for different  $\omega$  are plotted. The contour of constant energy density profile for  $\eta_m = 0.8$  has been plotted for reference. From Eqs. 7 and 5 one can deduce that the rapidity profile of baryon deposition due to the  $N_{coll}$  term is forward-backward symmetric in rapidity. On the other hand, the baryon deposited by the participant sources are asymmetric in rapidity as characterised by  $f_+^{n_B}$  and  $f_-^{n_B}$ . Now  $\omega$  controls the relative weight between the participant and binary collision sources. Thus, changing  $\omega$  amounts to changing the initial baryon tilt independent of the matter tilt.

In Figure 2, we have shown the effect of varying  $\omega$  on the initial rapidity profile of baryon density in panel (a) and in panel (b) the rapidity dependence of the baryon dipole asymmetry with respect to the centre of initial energy density.  $\eta_m$  is adjusted to ensure similar final state pion  $v_1$ . While the transverse coordinates integrated baryon rapidity profile does not show any dependency on  $\omega$ , the dipole asymmetry  $\varepsilon_1$  that characterises the first order harmonic in the Fourier expansion of the transverse distribution of baryon density shows large variation with  $\omega$ . The effect on the final state net baryon observables are shown in the lower row. In panel (c) we find the net proton rapidity profile is independent of  $\omega$  while in panel (d) we see that there is large variation in the  $v_1$  of  $p$  and  $\bar{p}$  affecting their mid-rapidity slopes as well as their splitting.

In a baryon free fireball, charged particle directed flow originates from initial tilted distribution of energy or entropy density in the reaction plane [2]. However, in a baryonic fireball it is possible to generate non-zero rapidity odd  $v_1$  of pion even with a forward-backward symmetric initial energy deposition but a tilted baryon profile. In panel (a) of Figure 3, we have demonstrated that how the directed flow of pion originates from tilted profile of baryon even when the energy density profile is symmetric in  $\eta_s$ . In this case the origin of pion  $v_1$  is the dipole asymmetry in pressure ( $p = p(\epsilon, n_B)$ ) in the transverse plane at non-zero rapidity which originates from the tilted baryon profile through EoS. This effect can be strong enough to generate sufficient pion  $v_1$  to explain data with just contribution from initial state pressure anisotropy. In panel(b) the effect on  $v_1(\pi^+)$  due to resonance decay and hadronic transport has been shown. It has been observed that the major contribution to  $v_1(\pi^+)$  comes from the effect of EoS while contribution from the resonance decay of higher baryons is very small. In the same plot, we have presented the effect of hadronic transport on the rapidity dependent directed flow.

## IV. RESULTS

We have studied Au+Au collisions at 19.6 GeV and 200 GeV. The simulations have been performed for both

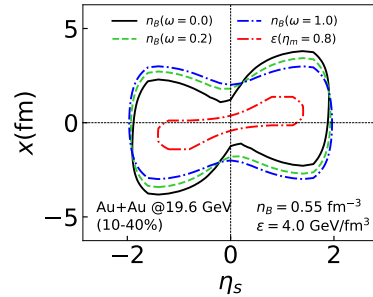


FIG. 1. (Color online) The contour plot of baryon profile with different  $\omega$ . Along the contour the baryon density is fixed to be  $0.55 \text{ fm}^{-3}$ .

$\sqrt{S_{NN}}$ (GeV)	$\tau_0$ (fm)	$\epsilon_0$ (GeV/fm <sup>3</sup> )	$\eta_0$	$\sigma_\eta$	$\eta_0^{n_B}$	$\sigma_{B,-}$	$\sigma_{B,+}$	$\omega$	$\eta_m$
$C_B = 0$									
200	0.6	8.0	1.3	1.5	4.4	2.0	0.1	0.3	2.0
19.6	1.8	1.55	1.3	0.4	1.5	0.9	0.3	0.13	0.8
$C_B = 1$									
200	0.6	8.0	1.3	1.5	4.6	1.6	0.1	0.25	2.2
19.6	1.8	1.55	1.3	0.4	1.8	0.8	0.3	0.15	0.8

TABLE I. Parameters used during simulations with  $C_B = 0$  and  $C_B = 1$ .

$C_B = 0$  and 1 to understand the effect of baryon diffusion on the presented observables. We have tuned our parameters to describe the available experimental data of the pseudo-rapidity dependence of charged particle multiplicity, centrality dependence of charged particle multiplicity, rapidity dependence of net proton yield and rapidity dependence of directed flow of identified hadrons simultaneously.

The centrality class has been determined from the initial state by assuming the produced charge particle multiplicity in the final stage is proportional to the two component ansatz of initial energy deposition in the transverse plane mentioned in Eq. 1. The hardness factor,  $\alpha$  has been chosen to capture the centrality dependence of charged particle yield in the mid rapidity region. We have found  $\alpha = 0.1$  and  $0.14$  is suitable for Au+Au collisions at 19.6 GeV and 200 GeV respectively.

We have observed that the pseudo rapidity dependence of charge particle multiplicity does not get affected by the  $\omega$  parameter although it mildly increases with  $C_B$ . However, the rapidity distribution of net proton is strongly affected by  $C_B$  due to different baryon diffusion. Hence we have first tuned and kept  $\epsilon_0, \eta_0$  and  $\sigma_\eta$  same for both  $C_B$  which describes the experimental data of pseudo rapidity dependent charge particle yield. In the second step, we have calibrated the  $\eta_0^{n_B}, \sigma_{B,in}$  and  $\sigma_{B,out}$  parameters independently for two different  $C_B$  values to explain the rapidity distribution of net proton yield. It is to be noted

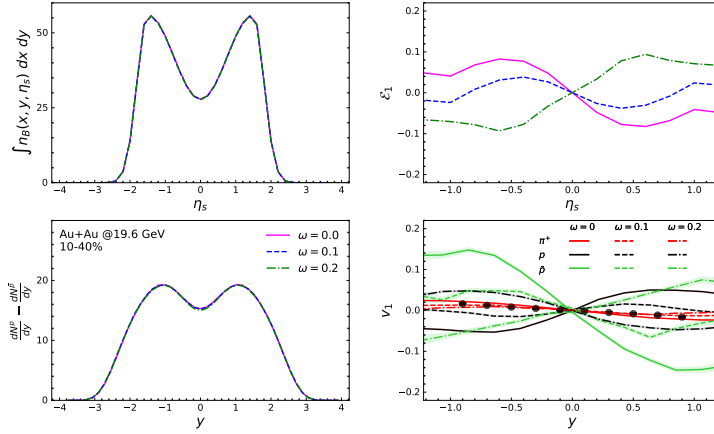


FIG. 2. (Color online) Effect of  $\omega$  proton and anti-proton directed flow split and the net proton rapidity distribution at 10-40% Au+Au  $\sqrt{s_{NN}} = 19.6$  GeV collisions. The experimental data of pion directed flow is measure by STAR collaboration [21].

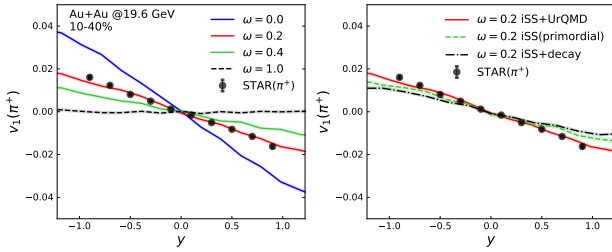


FIG. 3. (Color online) Effect of  $\omega$  on pion directed flow at 10-40% Au+Au  $\sqrt{s_{NN}} = 19.6$  GeV collisions. The experimental data of pion directed flow is measure by STAR collaboration [21].

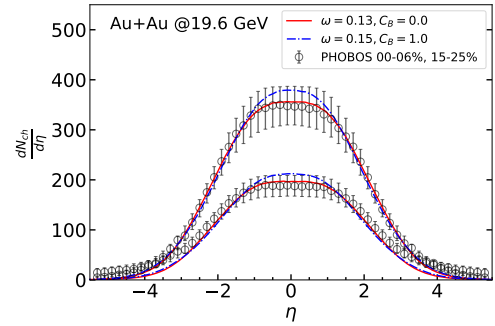


FIG. 4. (Color online) Pseudo rapidity distribution of produced charged particle for 0-6% and 15-25% centrality class in Au+Au collisions at  $\sqrt{s_{NN}} = 19.6$  GeV. The model expectations for both  $C_B = 0$  and 1 are compared to measurements from the PHOBOS collaboration [22].

here that, the weak decay contributions are taken into account during this calibrations.

The tilt parameter  $\eta_m$  controls the tilt in the energy density profile where as  $\omega$  controls the same for baryon density profile. We have observed that the presence of baryon density strongly affects the evolution of energy density inside the medium through EoS. Hence fixing of  $\eta_m$  and  $\omega$  indepently from the pion( $\pi$ ) and proton( $p$ ) directed flow is not possible. We have chosen a set of  $\omega - \eta_m$  for each  $C_B$  in order to explain the directed flow of  $\pi$ ,  $p$  and  $\bar{p}$  simultaneously.

Pseudo rapidity distribution of produced charged particle for 0-6% and 15-25% Au+Au collisions at  $\sqrt{s_{NN}} = 19.6$  GeV has been plotted in Fig. 4 for both  $C_B = 0$  and 1. There is a small increase in the charged particle yield in the case of  $C_B = 1$ . It is observed that the centrality dependence has been followed with the chosen hardness factor  $\alpha$ . Rapidity distribution of net proton for 0-5% and 10-20% centrality in Au+Au collisions at  $\sqrt{s_{NN}} = 19.6$

GeV have been plotted in Fig. 5. The weak decay contributions has been considered in the model calculation.

After constraining the model parameters of initial matter and baryon profile we have studied the phase space dependency of  $v_1$  of identified particles. Rapidity dependence of the directed flow of identified particles in 10-40% Au+Au collisions at  $\sqrt{s_{NN}} = 19.6$  have been plotted in Fig. 6. We have chosen a set of  $\eta_m$  and  $\omega$  to capture the rapidity dependence of  $v_1$  for  $\pi^+$ ,  $p$  and  $\bar{p}$  simultaneously whereas, the  $v_1$  of other particle species are the model predictions. From the model calculation it has been observed that both  $C_B = 0$  and  $C_B = 1$  are able to describe the baryon and anti-baryon  $v_1$  splitting at the measured rapidity range. So within the current scope of experimental measurements we are not able to constrain the  $C_B$ .

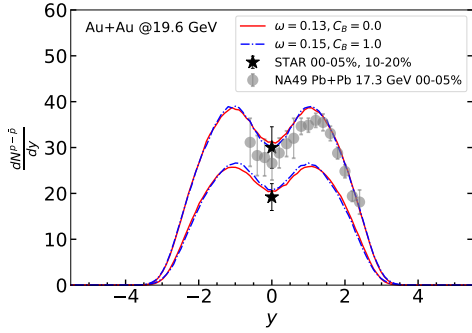


FIG. 5. (Color online) Rapidity distribution of net proton for 0-5% and 10-20% centrality class in Au+Au collisions at  $\sqrt{s_{NN}} = 19.6$  GeV. The model expectations for both  $C_B = 0$  and 1 are compared to experimental datas from NA49 [9] and STAR [1] collaboration. The NA49 data is for Pb+Pb  $\sqrt{s_{NN}} = 17.3$  GeV 0-5% centrality.

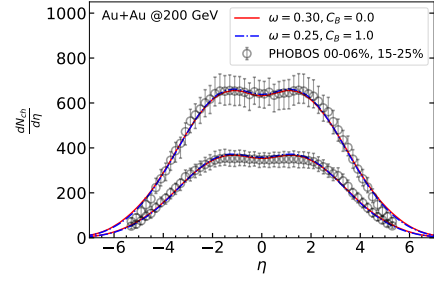


FIG. 7. (Color online) Pseudo rapidity distribution of produced charged particle for 0-6% and 15-25% centrality class in Au+Au collisions at  $\sqrt{s_{NN}} = 200$  GeV. The model expectations for both  $C_B = 0$  and 1 are compared to measurements from the PHOBOS collaboration [22].

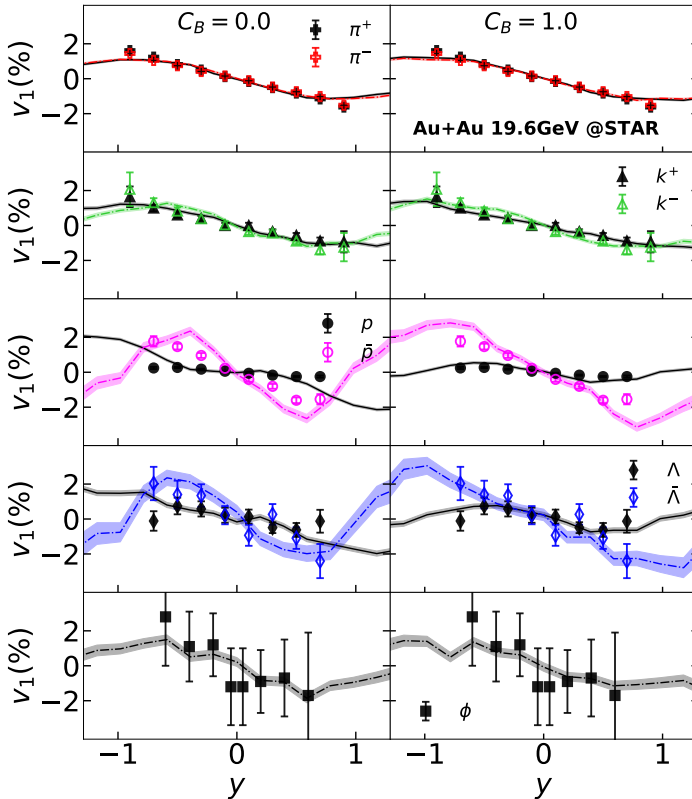


FIG. 6. (Color online) Phase space dependence of the rapidity odd directed flow of identified particles in 10-40% Au+Au collisions at  $\sqrt{s_{NN}} = 19.6$  GeV. The model results for both  $C_B = 0$  and 1 are compared with the measurements from STAR collaboration [21, 23].

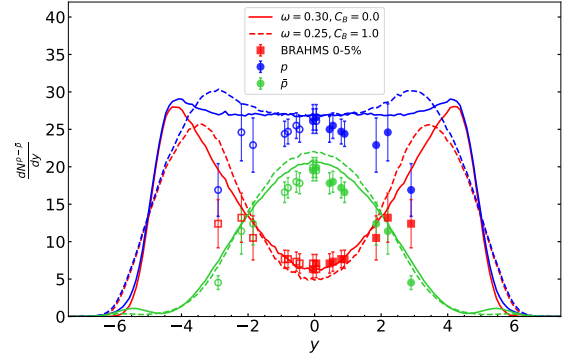


FIG. 8. (Color online) Rapidity distribution of net proton for 0-5% centrality class in Au+Au collisions at  $\sqrt{s_{NN}} = 200$  GeV. The model expectations for both  $C_B = 0$  and 1 are compared to measurements from the BRAHMS collaboration [7].

Pseudo rapidity distribution of produced charged particle for 0-6% and 15-25% Au+Au collisions at  $\sqrt{s_{NN}} = 200$  GeV has been plotted in Fig. 7 for both  $C_B = 0$  and 1. Rapidity distribution of net proton for 0-5% centrality class in Au+Au collisions at  $\sqrt{s_{NN}} = 200$  GeV has been plotted in Fig. 8. We are able to capture the proton, anti-proton and net-proton rapidity distribution which shows that the used freeze-out energy density gives a proper combination of  $T$  and  $\mu_B$  for the chemical equilibrium.

Rapidity dependence of the directed flow of identified particles in 10-40% Au+Au collisions at  $\sqrt{s_{NN}} = 200$  have been plotted in Fig. 9. There is relatively less splitting in baryon and anti-baryon at  $\sqrt{s_{NN}} = 200$  GeV as the net deposited baryon in mid-rapidity is very less.

We now revisit the issue of constraining  $C_B$  with  $v_1$ . We have seen so far that for rapidities upto 1 or 1.5, the model predictions for the different  $C_B$  are almost on top of each other and hence the data cannot discriminate between two different values of  $C_B$ . We have plotted in

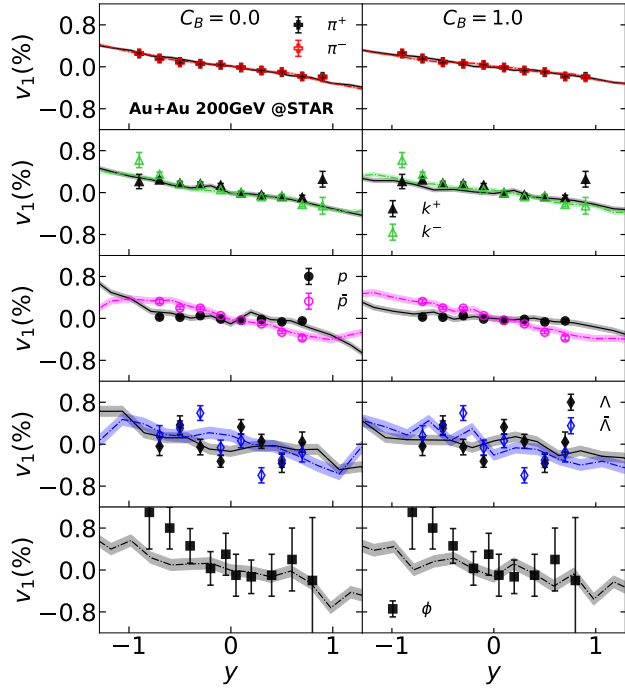


FIG. 9. (Color online) Phase space dependence of the rapidity odd directed flow of identified particles in 10-40% Au+Au collisions at  $\sqrt{s_{\text{NN}}} = 200$  GeV. The model results for both  $C_B = 0$  and 1 are compared with the measurements from STAR collaboration [21, 23].

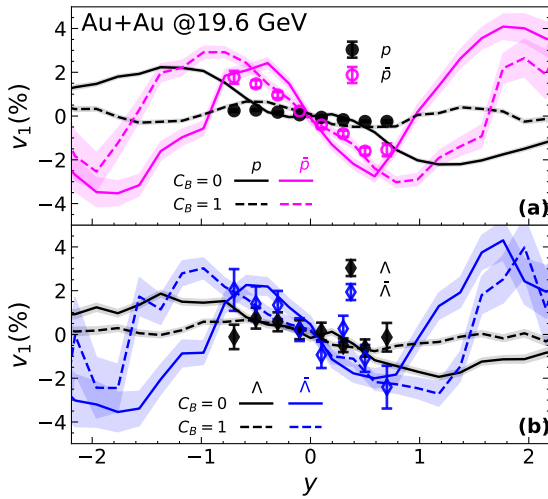


FIG. 10. (Color online) Phase space dependence of the rapidity odd directed flow of  $p, \Lambda$  and their anti-particles in 10-40% Au+Au collisions at  $\sqrt{s_{\text{NN}}} = 19.6$  GeV. The model results for both  $C_B = 0$  and 1 are compared with the measurements from STAR collaboration [21, 23].

Fig.. 10  $v_1$  over a large rapidity range. We find noticeable difference in the model calculation at large rapidity region that could be used to constrain  $C_B$  with the availability of such experimental data in the future.

## V. SUMMARY

We have studied the effect of baryon density on the identified particle directed flow. We have proposed a suitable initial transverse profile for the deposited baryon charge that allows us to study the interplay of matter and baryon tilt in the initial state and how subsequent hydrodynamic evolution of these conserved charges can help us to understand the identified particle directed flow in the Beam Energy Scan energies. Further, we demonstrated that  $v_1$  measurements at intermediate rapidities can provide strong constraints on the baryon diffusion coefficient.

- 
- [1] L. Adamczyk et al. (STAR), Phys. Rev. C **96**, 044904 (2017), arXiv:1701.07065 [nucl-ex].
- [2] P. Bozek and I. Wyskiel, Phys. Rev. C **81**, 054902 (2010), arXiv:1002.4999 [nucl-th].
- [3] C. Shen and S. Alzhvani, Phys. Rev. C **102**, 014909 (2020), arXiv:2003.05852 [nucl-th].
- [4] S. Jeon and J. I. Kapusta, Phys. Rev. C **56**, 468 (1997), arXiv:nucl-th/9703033.
- [5] A. De, J. I. Kapusta, M. Singh, and T. Welle, Phys. Rev. C **106**, 054906 (2022), arXiv:2206.02655 [nucl-th].
- [6] G. S. Denicol, C. Gale, S. Jeon, A. Monnai, B. Schenke, and C. Shen, Phys. Rev. C **98**, 034916 (2018), arXiv:1804.10557 [nucl-th].
- [7] I. G. Bearden et al. (BRAHMS), Phys. Rev. Lett. **93**, 102301 (2004), arXiv:nucl-ex/0312023.
- [8] I. C. Arsene et al. (BRAHMS), Phys. Lett. B **677**, 267 (2009), arXiv:0901.0872 [nucl-ex].
- [9] T. Anticic et al. (NA49), Phys. Rev. C **83**, 014901 (2011), arXiv:1009.1747 [nucl-ex].
- [10] B. Schenke, S. Jeon, and C. Gale, Phys. Rev. C **82**, 014903 (2010), arXiv:1004.1408 [hep-ph].
- [11] J.-F. Paquet, C. Shen, G. S. Denicol, M. Luzum, B. Schenke, S. Jeon, and C. Gale, Phys. Rev. C **93**, 044906 (2016), arXiv:1509.06738 [hep-ph].
- [12] B. Schenke, S. Jeon, and C. Gale, Phys. Rev. C **85**, 024901 (2012), arXiv:1109.6289 [hep-ph].
- [13] A. Monnai, B. Schenke, and C. Shen, Phys. Rev. C **100**, 024907 (2019), arXiv:1902.05095 [nucl-th].
- [14] A. Bazavov et al. (HotQCD), Phys. Rev. D **86**, 034509 (2012), arXiv:1203.0784 [hep-lat].
- [15] H. T. Ding, S. Mukherjee, H. Ohno, P. Petreczky, and H. P. Schadler, Phys. Rev. D **92**, 074043 (2015), arXiv:1507.06637 [hep-lat].
- [16] A. Bazavov et al., Phys. Rev. D **95**, 054504 (2017), arXiv:1701.04325 [hep-lat].
- [17] C. Shen, Z. Qiu, H. Song, J. Bernhard, S. Bass, and U. Heinz, “The iebe-vishnu code package for relativistic heavy-ion collisions,” (2014).
- [18] “The iSS code package can be downloaded from <https://github.com/chunshen1987/iSS>,” .
- [19] S. A. Bass et al., Prog. Part. Nucl. Phys. **41**, 255 (1998), arXiv:nucl-th/9803035.
- [20] M. Bleicher et al., J. Phys. G **25**, 1859 (1999), arXiv:hep-ph/9909407.
- [21] L. Adamczyk et al. (STAR), Phys. Rev. Lett. **112**, 162301 (2014), arXiv:1401.3043 [nucl-ex].
- [22] B. B. Back et al., Phys. Rev. Lett. **91**, 052303 (2003), arXiv:nucl-ex/0210015.
- [23] L. Adamczyk et al. (STAR), Phys. Rev. Lett. **120**, 062301 (2018), arXiv:1708.07132 [hep-ex].